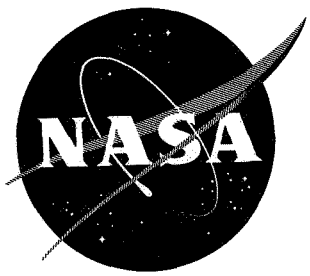

TECHNICAL MEMORANDUM

X - 68

SOME EXPERIMENTAL HEATING DATA ON A 5.0-INCH-DIAMETER FLAT FACE WITH HEMISPHERICAL DEPRESSIONS

By Thomas W. Tyner

Langley Research Center
Langley Field, Va.

NATIONAL AERONAUTICS AND SPACE ADMINISTRATION

WASHINGTON

September 1959

NATIONAL AERONAUTICS AND SPACE ADMINISTRATION

TECHNICAL MEMORANDUM X-68

SOME EXPERIMENTAL HEATING DATA ON A 5.0-INCH-DIAMETER FLAT FACE WITH HEMISPHERICAL DEPRESSIONS*

By Thomas W. Tyner

SUMMARY

A flat-faced cone, 5.0 inches in diameter with four hemispherical depressions, was flight tested to obtain heat-transfer data. The data were reduced at Mach numbers of 5.0 and 6.3 and Reynolds numbers per foot of 25.54×10^6 and 29.93×10^6, respectively. The results indicate an increase in heating rate up to 93 percent at the depressions.

INTRODUCTION

The National Aeronautics and Space Administration is interested in blunt-nose shapes for reentry applications, and recent research has shown that the flat face is a promising configuration because of its lower stagnation-point heat transfer and lower total heat input during laminar-flow conditions. Possible use of a flat face as the nose on reentry vehicles raises the question of the possible effects of damage from countermeasures or meteoroids. Therefore, the Langley Pilotless Aircraft Research Division has conducted investigations to determine the local heating about simulated damage points in the form of hemispherical depressions. The data presented in this paper are the result of a flight test made at the NASA Wallops Station by using a propulsion system consisting of two stages of solid-propellant rocket motors; the first stage was a Nike booster (M5 JATO) and the sustainer was a Recruit motor (JATO XM19 E1). The test configuration was a $14\frac{1}{2}^\circ$ half-angle truncated cone with a 5.0-inch-diameter flat face. The flat face was indented with four hemispherical depressions of various sizes placed at various stations. The data are presented primarily for Mach numbers of 5.0 and 6.3 and Reynolds numbers per foot of 25.54×10^6 and 29.93×10^6, respectively.

*Title, Unclassified.

SYMBOLS

c_p	specific heat, Btu/(lb)(^oR)
M	Mach number
q	heating rate, Btu/(sq ft)(sec)
r	radius, ft
T	temperature, ^oR
t	time, sec
x	radial distance from stagnation point, ft
ρ	density, lb/cu ft
τ	thickness, ft

Subscripts:

t	stagnation conditions
w	conditions at wall

Abbreviations:

TC.	thermocouple
EQ. SP.	equally spaced (see fig. 6)

MODEL AND TEST

Model

Figure 1 shows a dimensioned sketch of the model and booster system, and figure 2 shows the general configuration of the model on the launcher. The propulsion system consisted of a Nike booster, stabilized by four $2\frac{1}{2}$-square-foot fins, and a Recruit sustainer, stabilized by a 10^o half-angle flare.

Figures 3, 4, and 5 show detailed views of the nose. The telemeter and batteries are contained in a cone-cylinder section just ahead of the Recruit motor.

The flat face was made from 0.050-inch-thick Inconel and was finished to a surface roughness of 6 microinches as measured by a profilometer. Actual skin-thickness measurements made at each thermocouple location are presented in table I. The nose was supported in compression by a ribbed, mild steel form coated with aluminum oxide for insulation purposes. The configuration was a truncated cone 2.258 inches long with a semivertex angle of 14.5°, a base diameter of 6.424 inches, and a tip diameter of 5.0 inches.

The flat face of the model was impressed with four hemispherical depressions. Three of the depressions had a radius of 0.25 inch and were placed at stations x/r of 0.333, 0.667, and 1.00. The fourth depression, with a radius of 0.50 inch, was placed at a station x/r of 0.677. Details of this model are shown in figure 6.

Instrumentation

The model was equipped with four channels of telemetry, two of which were devoted to thermocouples and the other two were devoted to longitudinal accelerometers. The flat face of the model was instrumented with 18 thermocouples, 6 in a ray extending out from the center on one channel and 12 in the various depressions on the second channel. All thermocouples were No. 30 chromel-alumel wire and were welded to the inside surface of the flat face. The entire thermocouple arrangement is shown in figure 6.

This model was also instrumented with two longitudinal accelometers to supply velocity and drag data. However, satisfactory velocity data were obtained by a CW Doppler radar set, and no drag data were received because of telemeter failure.

Just prior to launching the flight model, atmospheric conditions were measured by means of radiosondes that were tracked by a Rawin set AN/GMD-1A. Model velocities were obtained with a CW Doppler radar set, and the space-time coordinates were plotted by an NASA modified SCR-584 radar set.

Flight Test

The model was launched at an elevation angle of 60°. The Nike motor boosted the model to a Mach number of 2.71 at 3.5 seconds, and the Recruit motor accelerated it to a Mach number of 7 at 5.8 seconds. Figure 7 shows

the time histories of Mach number, altitude, and Reynolds number for this model.

Temperature data were received from zero time to 6.0 seconds, at which time the telemeters failed. It should be noted that at the time of the telemeter failure, the model skin temperature was nearly at the melting point of Inconel. It is possible that this in conjunction with high airloads caused the telemeter failure.

DATA REDUCTION

The variation of the measured skin temperatures with time is presented in figure 8. These curves are arranged in groups for comparison of the temperatures on the flat face or in the depressions. The temperature scales of figure 8 are staggered to allow vertical separation of the curves.

The heating rates presented in figure 9 were calculated for each thermocouple location by using the formula

$$q = \left(c_p \rho \tau\right)_w \frac{dT_w}{dt}$$

The value dT_w/dt was determined from the temperature history of the model. This value was then plotted and a smooth curve was faired through the points. Radiation and conduction effects were estimated and found to be negligible for the times considered.

No pressure measurements were made on this model; however, the pressure distribution and the velocity for a flat face as given in reference 1 were assumed to hold here. This was felt to be a reasonable assumption since these parameters are essentially invariant with Mach number above a Mach number of approximately 2.

A time history of the heating rate reduced from the temperature time histories and presented for the time interval of 4 seconds to telemeter failure is given for each thermocouple location in figure 9. Theoretical values for the laminar heating ratio q/q_t were calculated from the theory given in reference 2 by using the nondimensional temperature parameter as given in reference 3.

The theoretical heating rate for turbulent flow was calculated from reference 4 by using the theory of reference 5. For these calculations, the adiabatic-wall temperature was assumed to be constant over the flat

face. Actually it varied less than 1 percent from the stagnation point to the station of thermocouple 6.

RESULTS AND DISCUSSION

Figure 10 presents values of q/q_t at Mach numbers of 5 and 6.3 for each thermocouple location along with the theoretical values for laminar and turbulent flow along a smooth flat face. The heating rates calculated from the ray of thermocouples along the flat face fall on or below the theoretical laminar-flow curve. Thus, it is probable that in the absence of the depressions, flow over the entire face would have been laminar. The heating rates in the hemispherical depressions indicate transitional and turbulent flow.

The experimental results show that, although the heating rates in the depressions nearest the stagnation point are lower than those in the pits near the edge of the model, the flow is more nearly turbulent about the inboard pit than about the outboard pit. This can be seen from figure 10 by comparing the data points with the turbulent-theory curve at x/r stations less than 0.5 and by comparing data points with the theory curve at x/r stations greater than 0.5.

The behavior of the heating rates in the depressions on this model contrasts greatly with the behavior in pits at the stagnation point. Reference 6 shows the heat-transfer coefficient at the bottom of a hemispherical pit at the stagnation point of a cone-hemisphere nose to be one-tenth the stagnation value of a smooth hemispherical nose at a Mach number of 8. Reference 7 shows that the heat-transfer coefficient at the bottom of a hemispherically concave nose is about 0.08 of the stagnation value of a hemispherically convex nose of the same diameter. Some unpublished data obtained at the Langley Research Center from the ceramic-heated jet (pilot model) on flat-face models with cylindrical pits at the stagnation points also show that depressions at the stagnation point reduce the heating rate.

CONCLUSIONS

From the experimental data presented, the following conclusions may be drawn:

1. Flow over the face of the model was basically laminar.

2. Depressions on the nose tripped the boundary layer and caused higher local heating corresponding to either transitional or turbulent flow.

3. The measured heating rates indicated that the flow about the inboard depression was more nearly turbulent than that about the outboard depression.

Langley Research Center,
National Aeronautics and Space Administration,
Langley Field, Va., June 29, 1959.

L
5
4
3

REFERENCES

1. Maccoll, J. W., and Codd, J.: Theoretical Investigations of the Flow Around Various Bodies in the Sonic Region of Velocities. British Theor. Res. Rep. No. 17/45, B.A.R.C. 45/19, Armament Res. Dept., Ministry of Supply, 1945.

2. Stine, Howard A., and Wanlass, Kent: Theoretical and Experimental Investigation of Aerodynamic-Heating and Isothermal Heat-Transfer Parameters on a Hemispherical Nose With Laminar Boundary Layer at Supersonic Mach Numbers. NACA TN 3344, 1954.

3. Levy, Solomon: Heat Transfer to Constant-Property Laminar Boundary-Layer Flows With Power-Function Free-Stream Velocity and Wall-Temperature Variation. Jour. Aero. Sci., vol. 19, no. 5, May 1952, pp. 341-348.

4. Stoney, William E., Jr., and Markley, J. Thomas: Heat Transfer and Pressure Measurements on Flat-Faced Cylinders at Mach Number 2. NACA TN 4300, 1958.

5. Van Driest, E. R.: The Problem of Aerodynamic Heating. Aero. Eng. Rev., vol. 15, no. 10, Oct. 1956, pp. 26-41.

6. Hopko, Russell N., and Strass, H. Kurt: Some Experimental Heating Data on Convex and Concave Hemispherical Nose Shapes and Hemispherical Depressions on a 30° Blunted Nose Cone. NACA RM L58A17a, 1958.

7. Levine, Jack, and Rumsey, Charles B.: Heat-Transfer Measurements on a 5.5-Inch-Diameter Hemispherical Concave Nose in Free Flight at Mach Numbers up to 6.6. NASA MEMO 10-21-58L, 1958.

TABLE I

SKIN THICKNESS AT THERMOCOUPLE LOCATIONS

Thermocouple	x/r	Skin thickness, in.	Thermocouple	x/r	Skin thickness, in.
1	0	0.049	10	0.667	0.055
2	.1667	.051	11	.808	.055
3	.333	.051	12	.682	.055
4	.500	.050	13	.595	.059
5	.667	.051	14	.667	.057
6	.833	.050	15	.737	.059
7	.920	.059	16	.263	.059
8	.965	.057	17	.333	.057
9	.526	.055	18	.404	.059

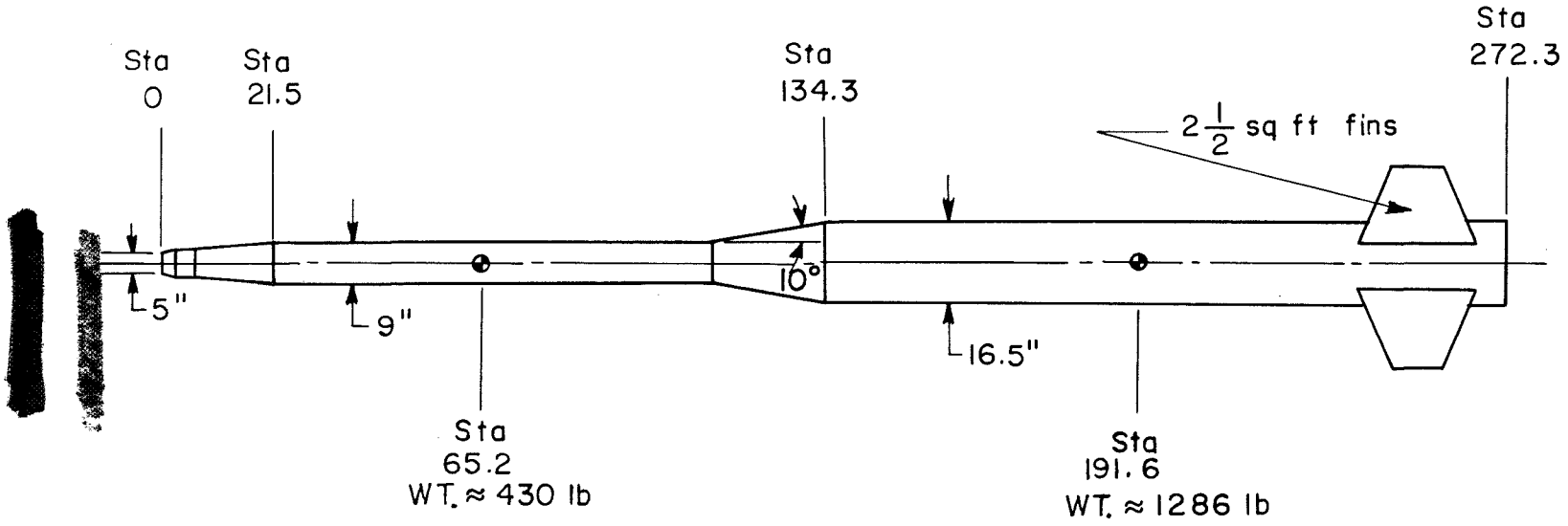

Figure 1.- Model and booster system. All dimensions are in inches.

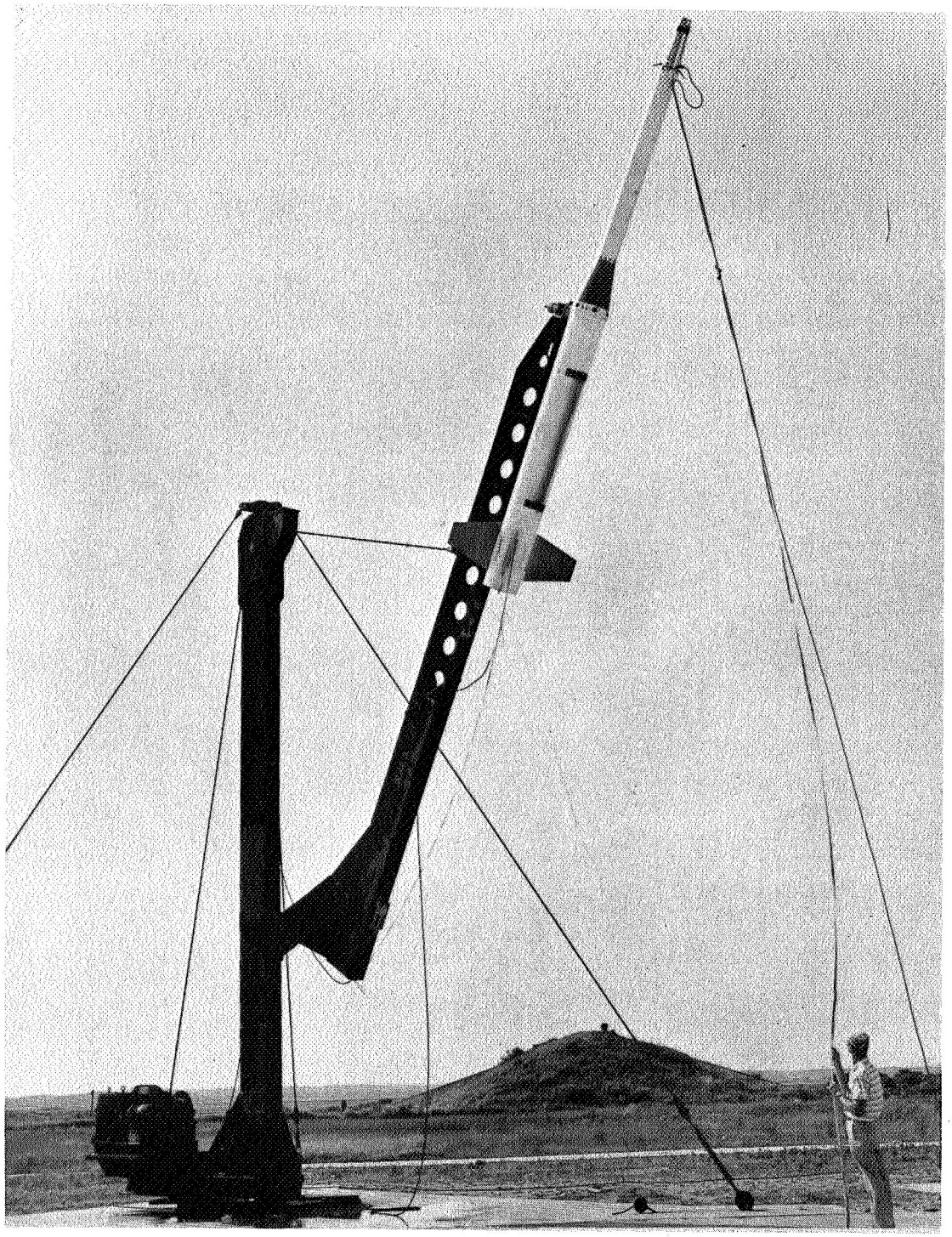

Figure 2.- Model on launcher. L-58-3456

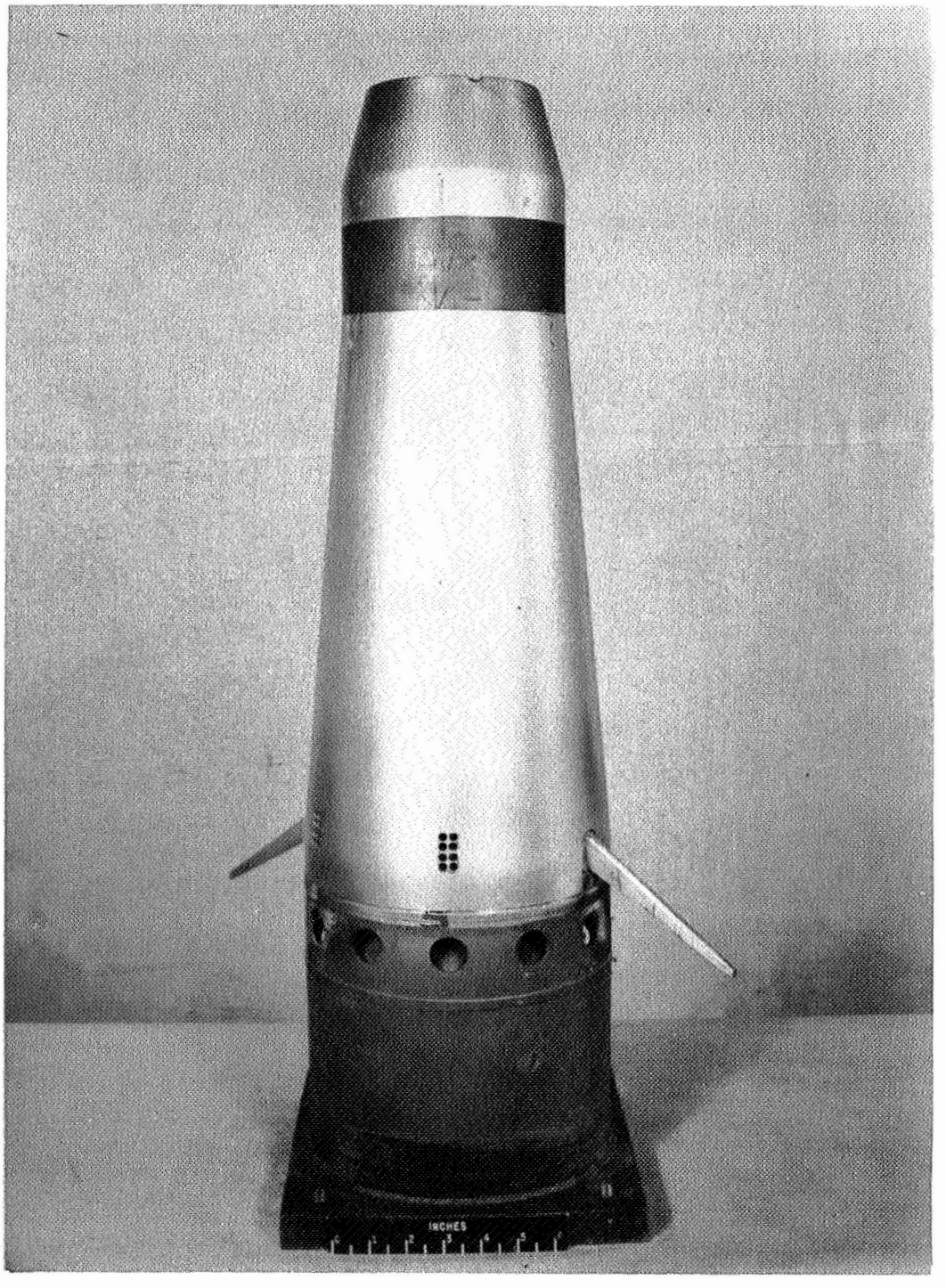

Figure 3.- Side view of model. L-58-3159.1

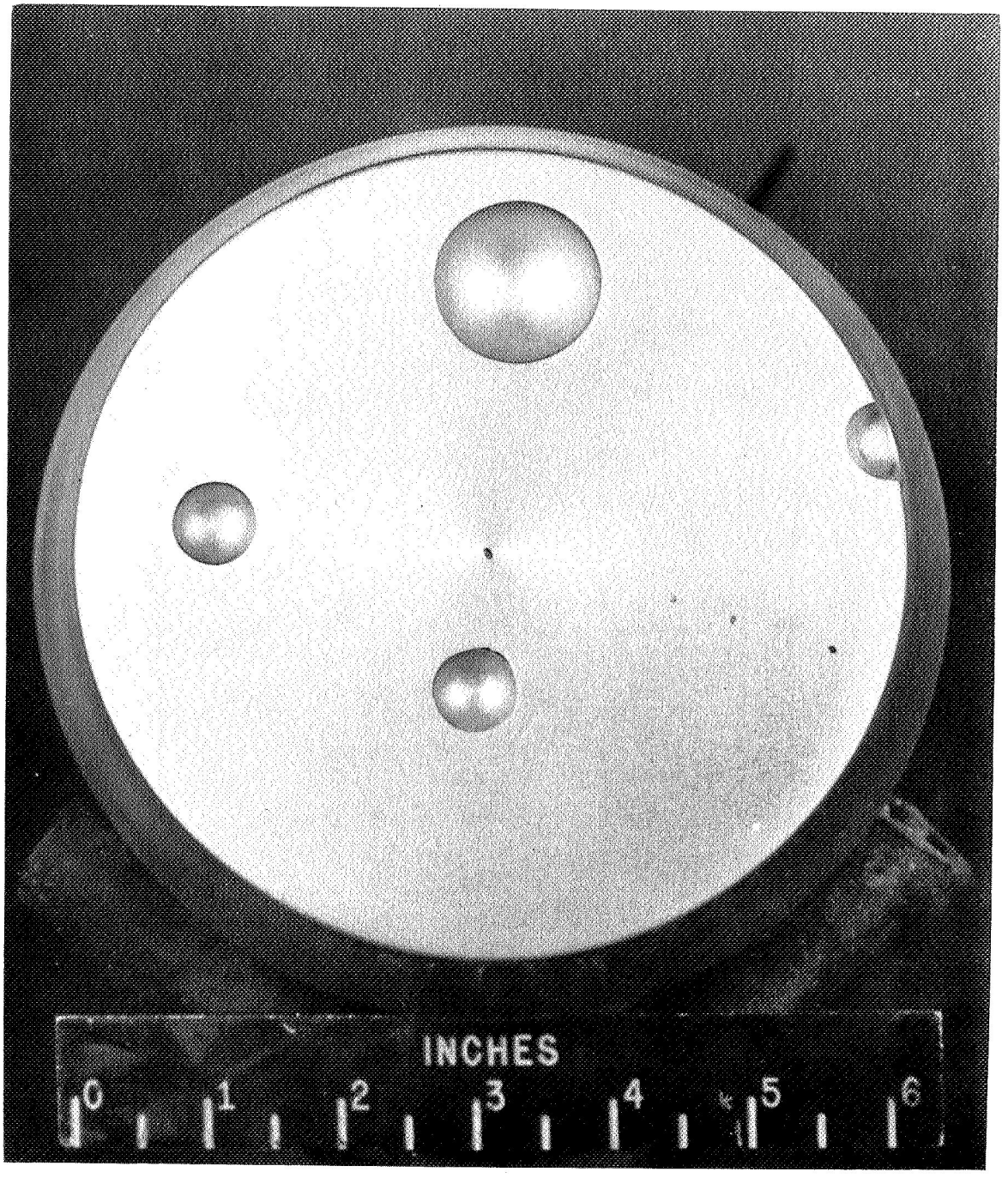

Figure 4.- Front view of model. L-58-3160

L-345

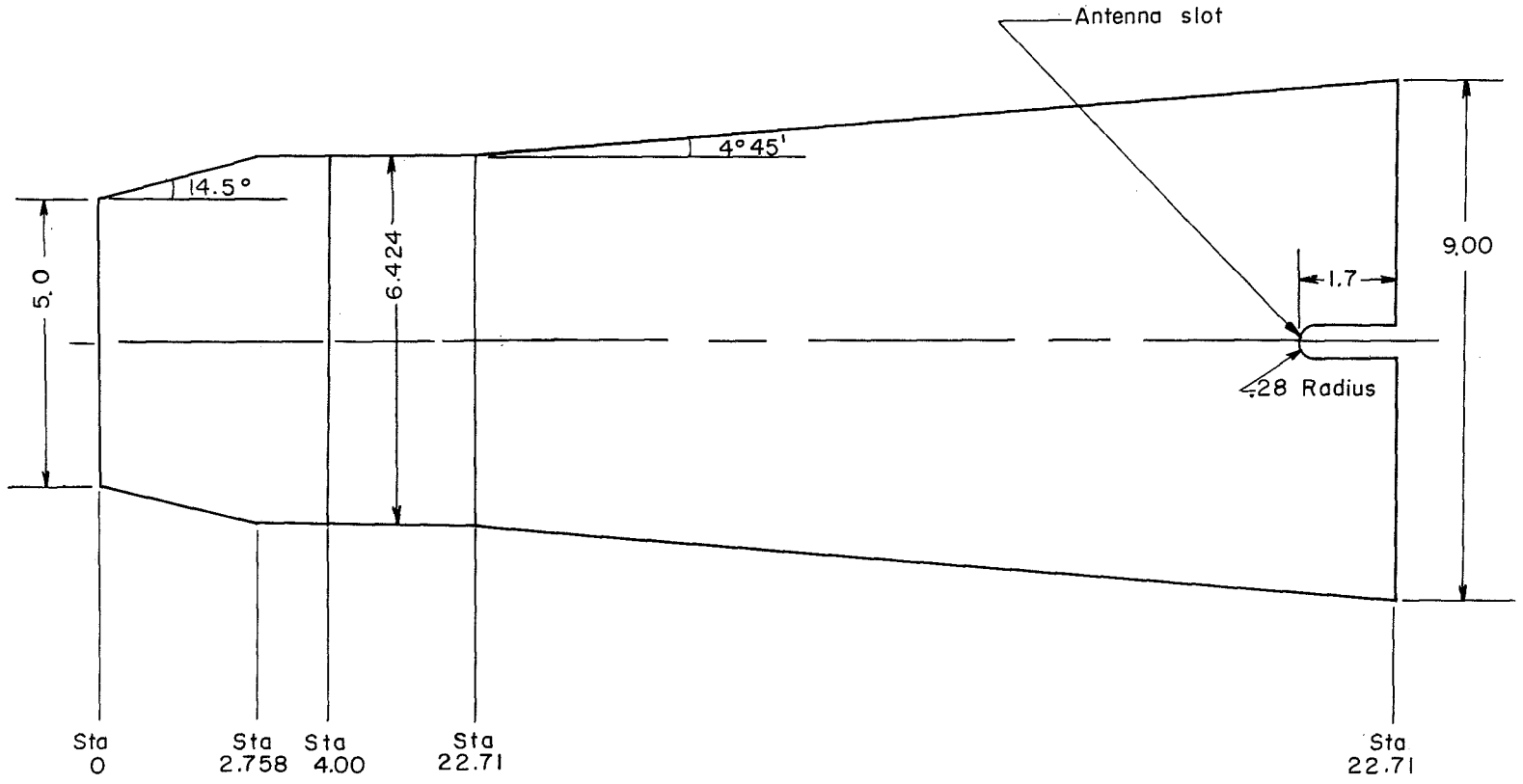

Figure 5.- Nose cone and telemeter housing. All dimensions are in inches.

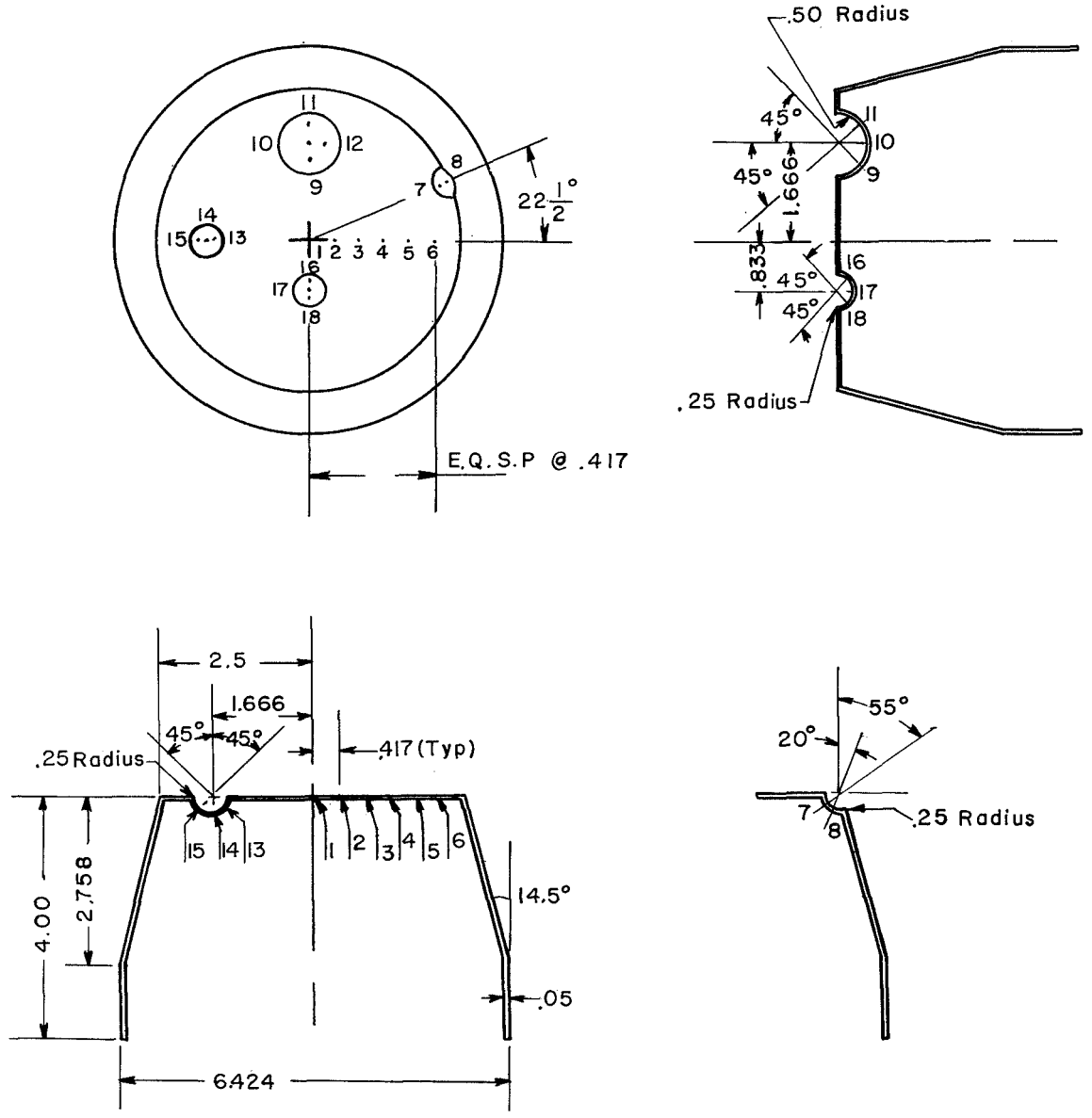

Figure 6.- Thermocouple layout of model. All dimensions are in inches.

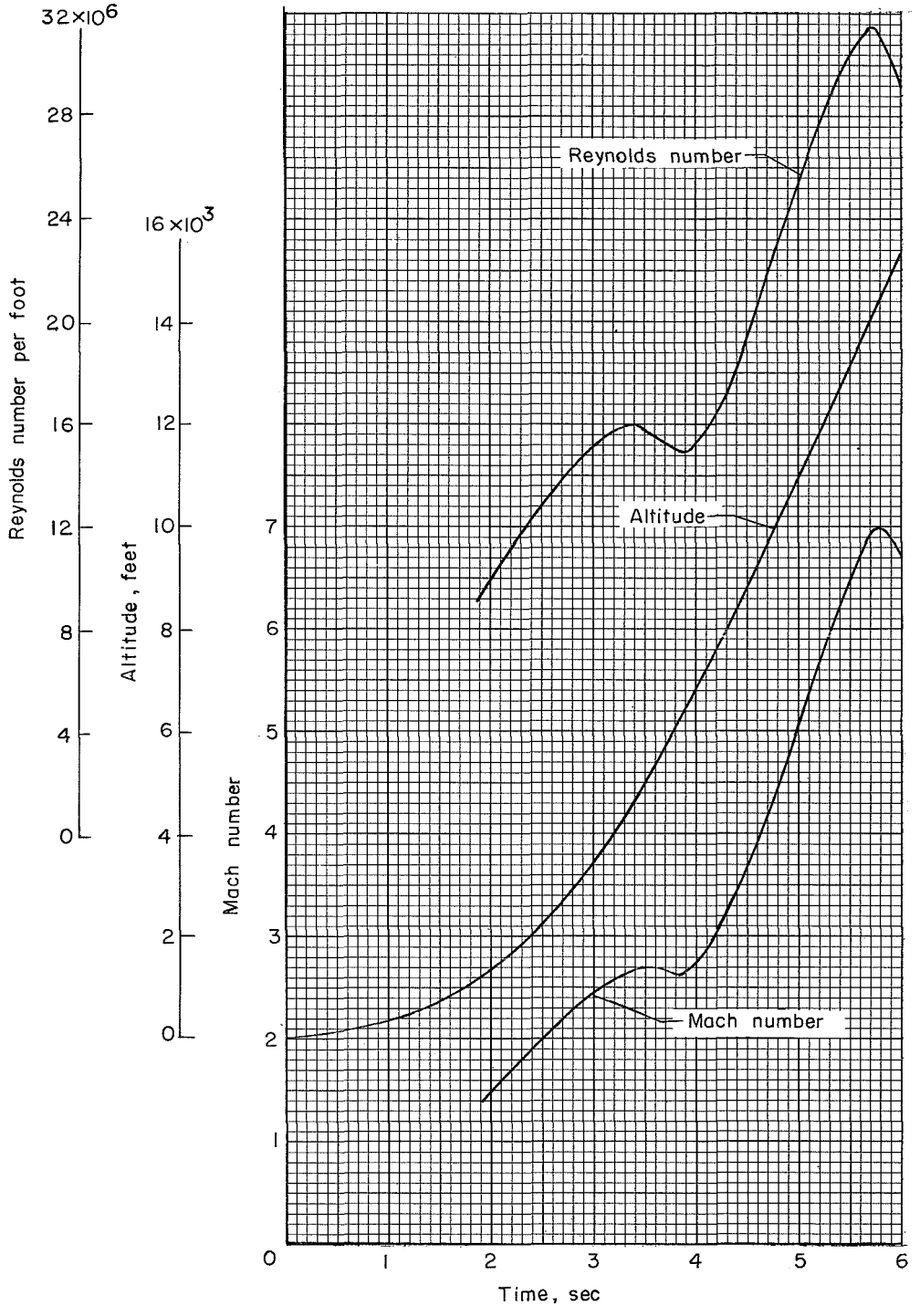

Figure 7.- Variation of Mach number, altitude, and Reynolds number with time.

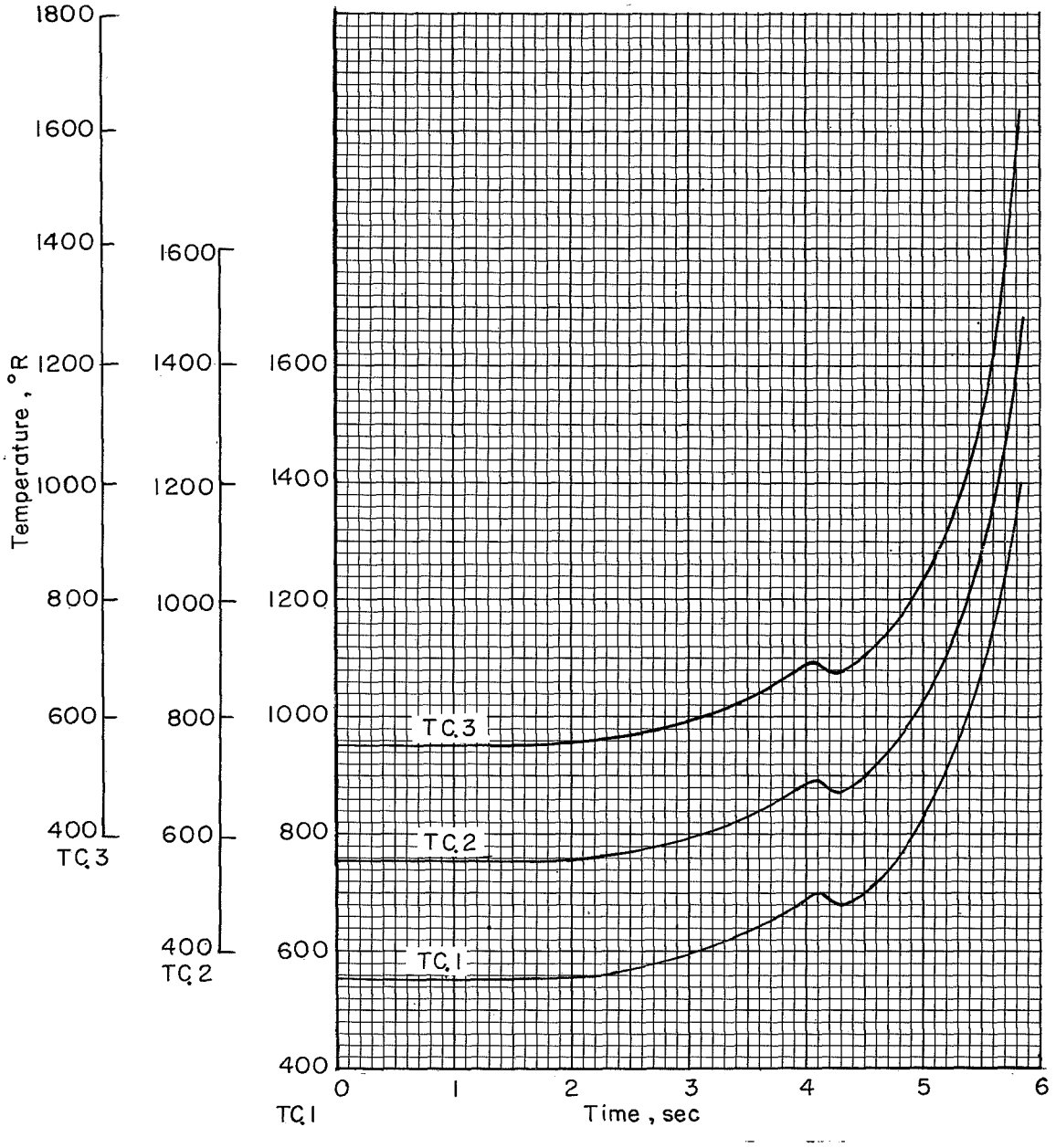

(a) Thermocouples 1, 2, and 3.

Figure 8.- Variation of skin temperature with time.

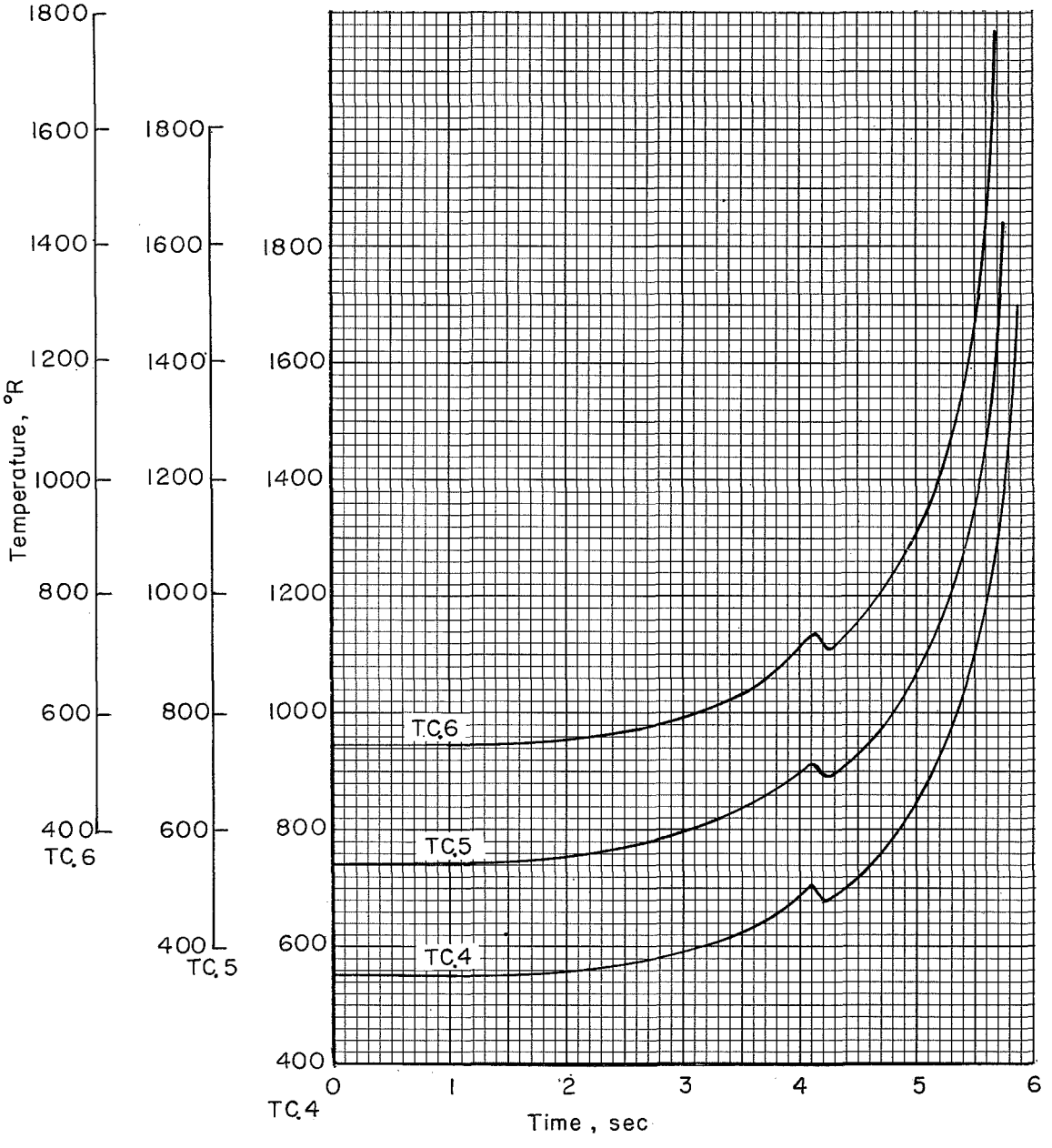

(b) Thermocouples 4, 5, and 6.

Figure 8.- Continued.

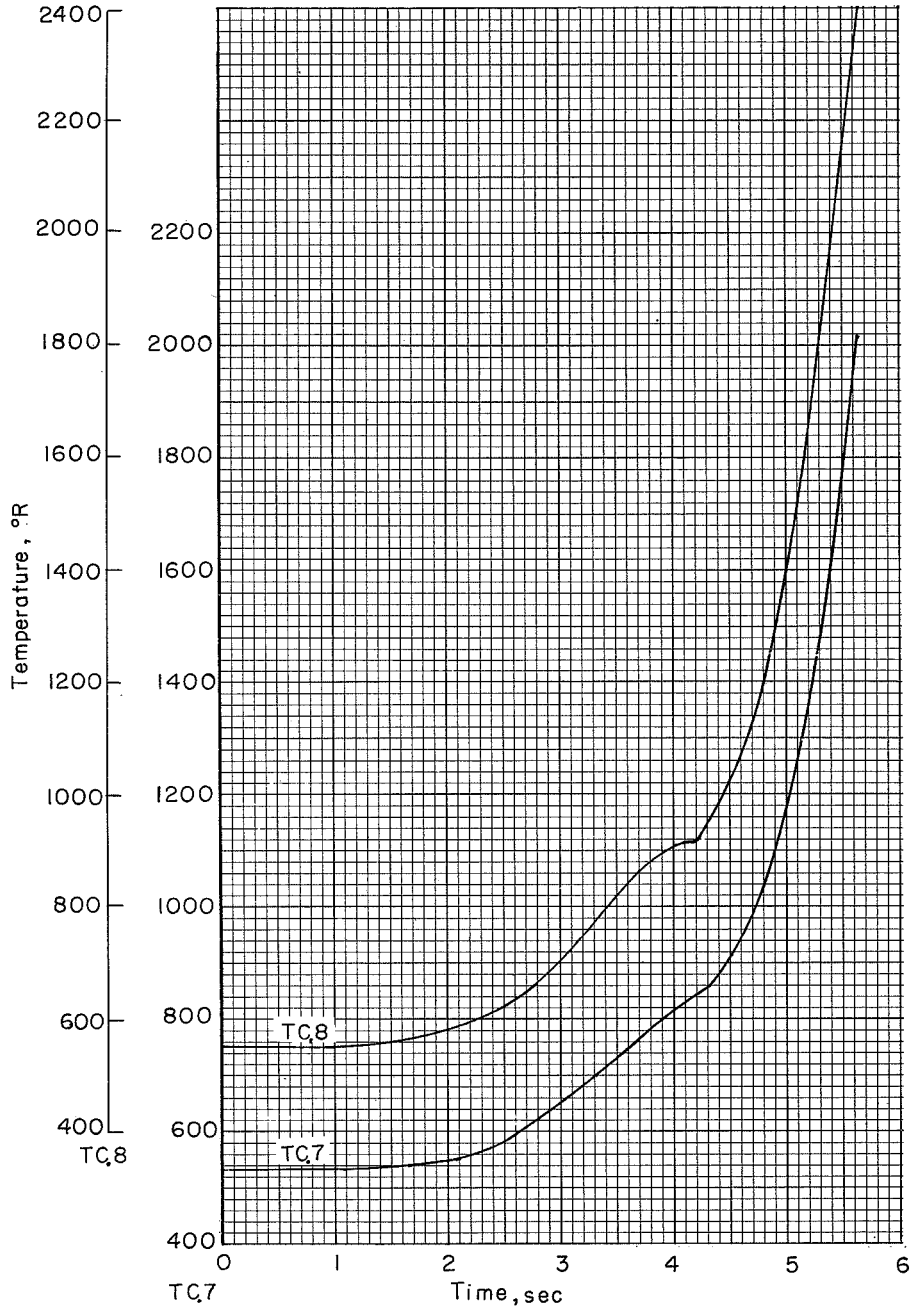

(c) Thermocouples 7 and 8.

Figure 8.- Continued.

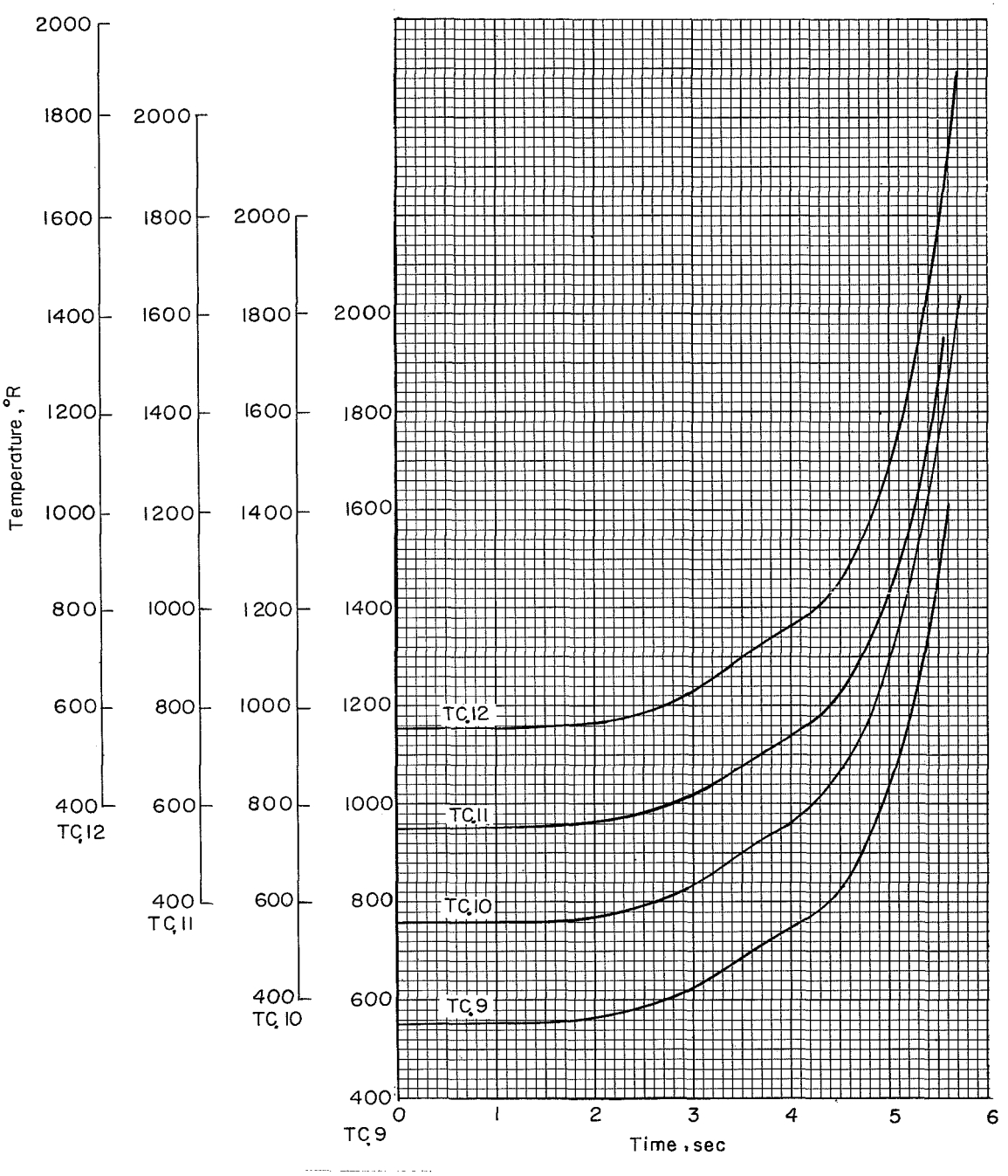

(d) Thermocouples 9 to 12.

Figure 8.- Continued.

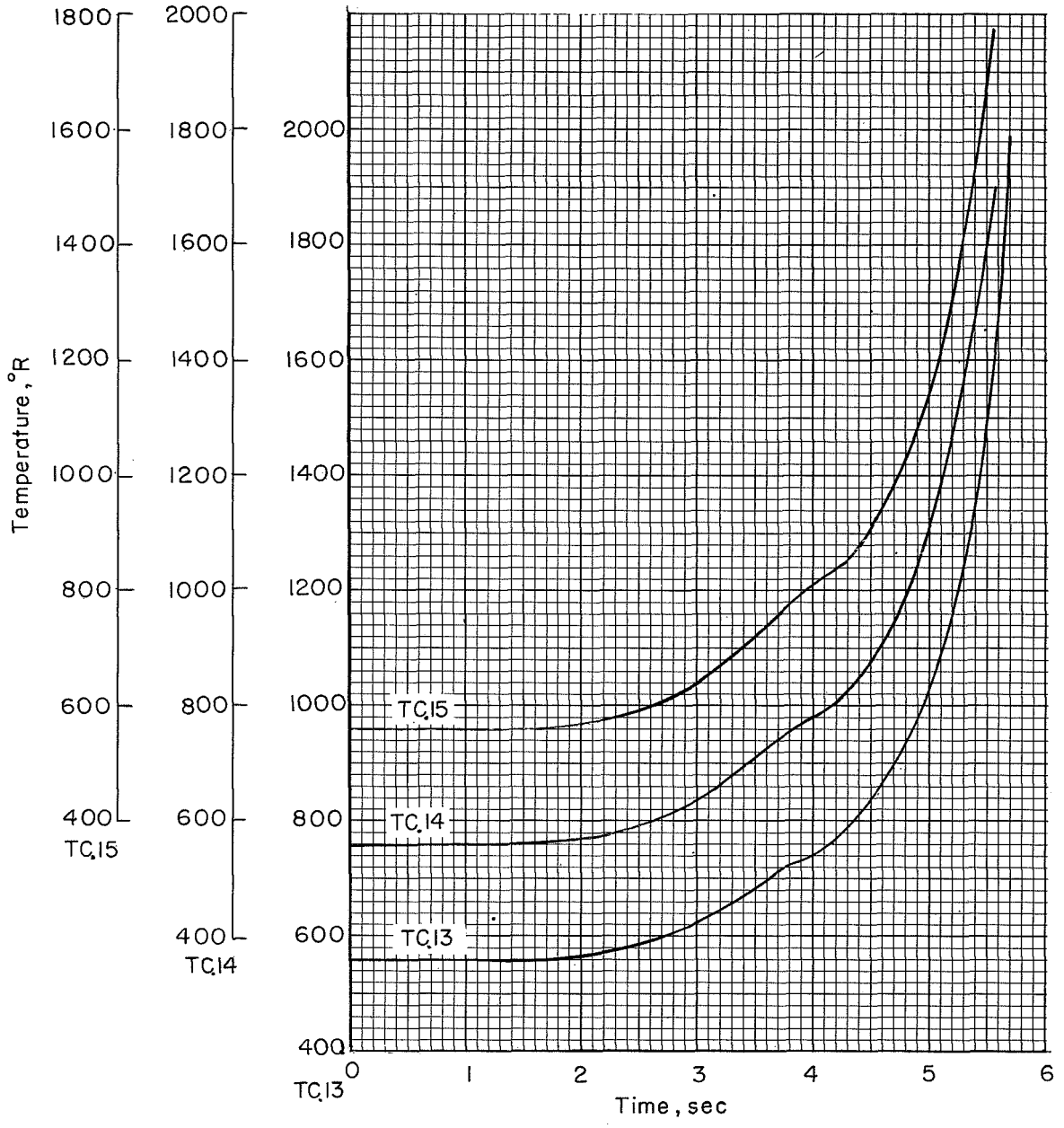

(e) Thermocouples 13, 14, and 15.

Figure 8.- Continued.

L-543

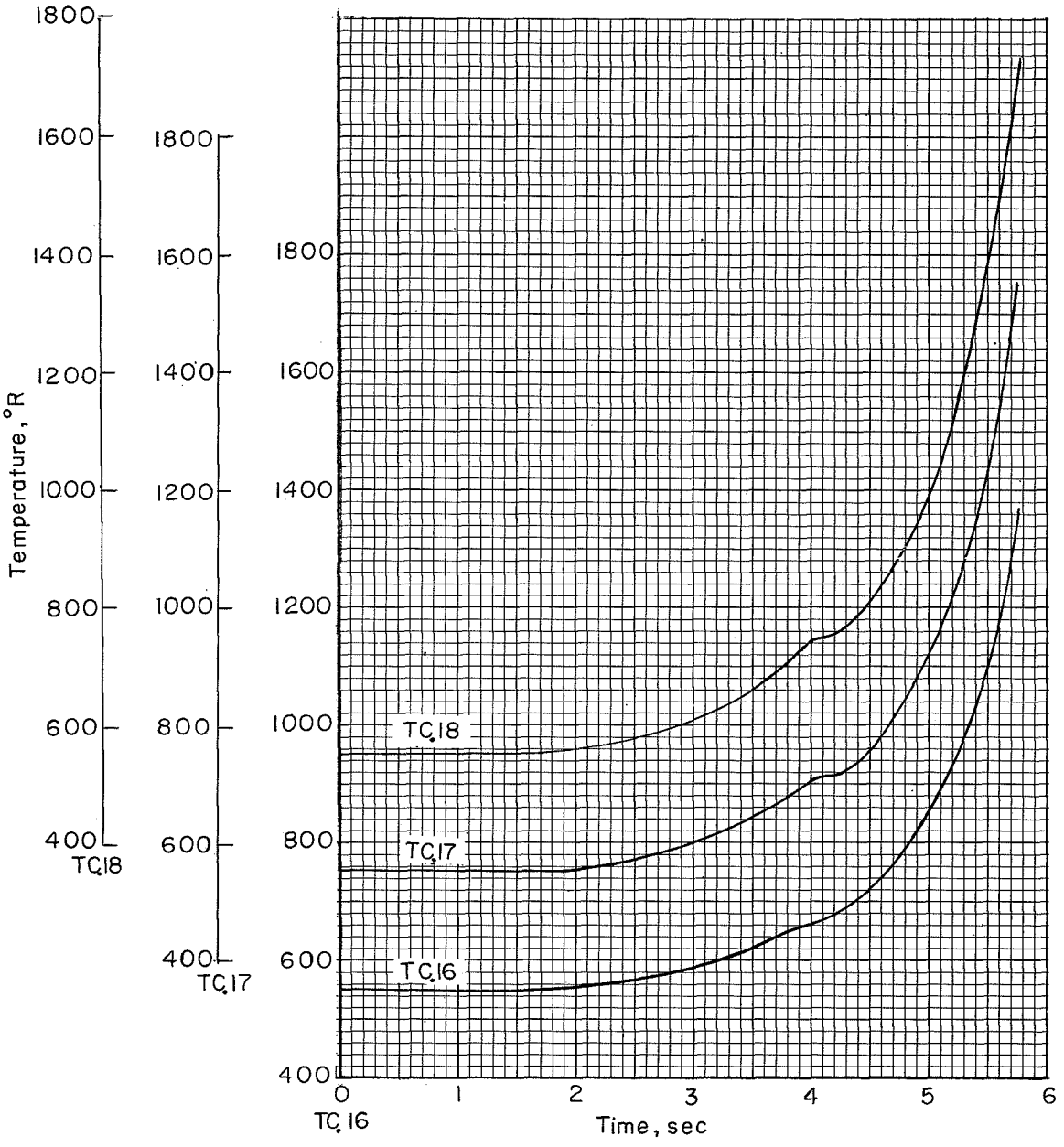

(f) Thermocouples 16, 17, and 18.

Figure 8.- Concluded.

L-543

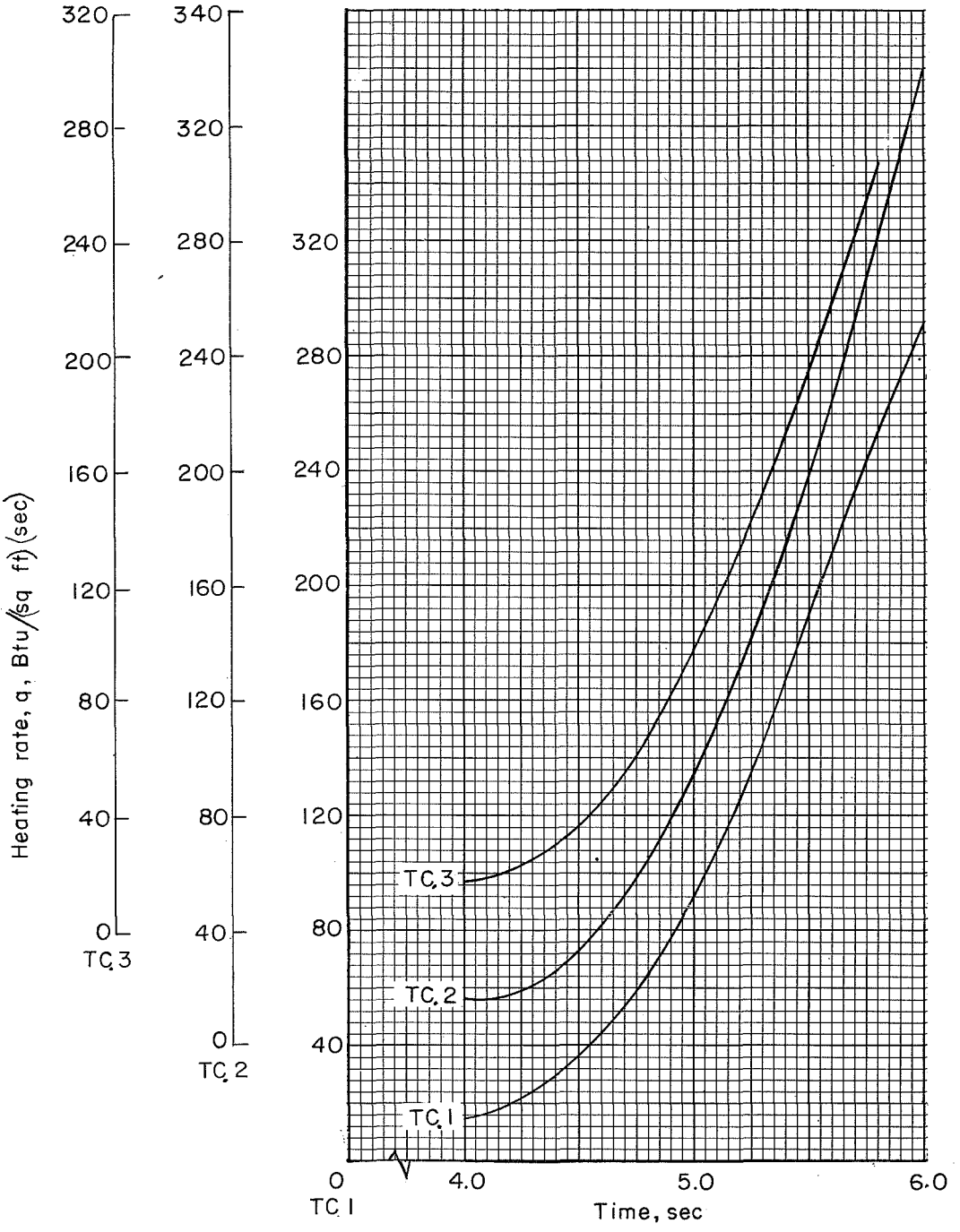

(a) Thermocouples 1, 2, and 3.

Figure 9.- Variation of heating rates with time.

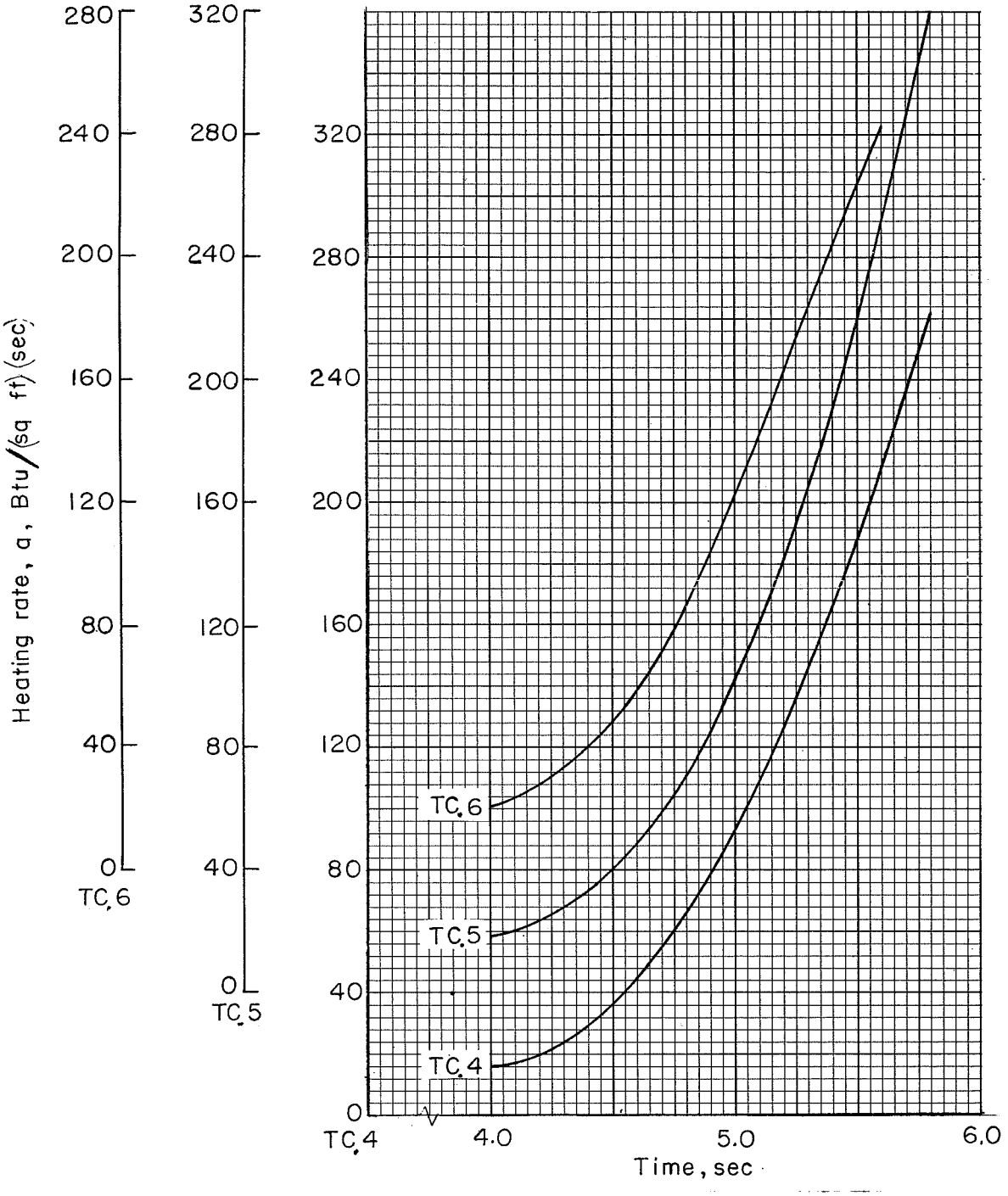

(b) Thermocouples 4, 5, and 6.

Figure 9.- Continued.

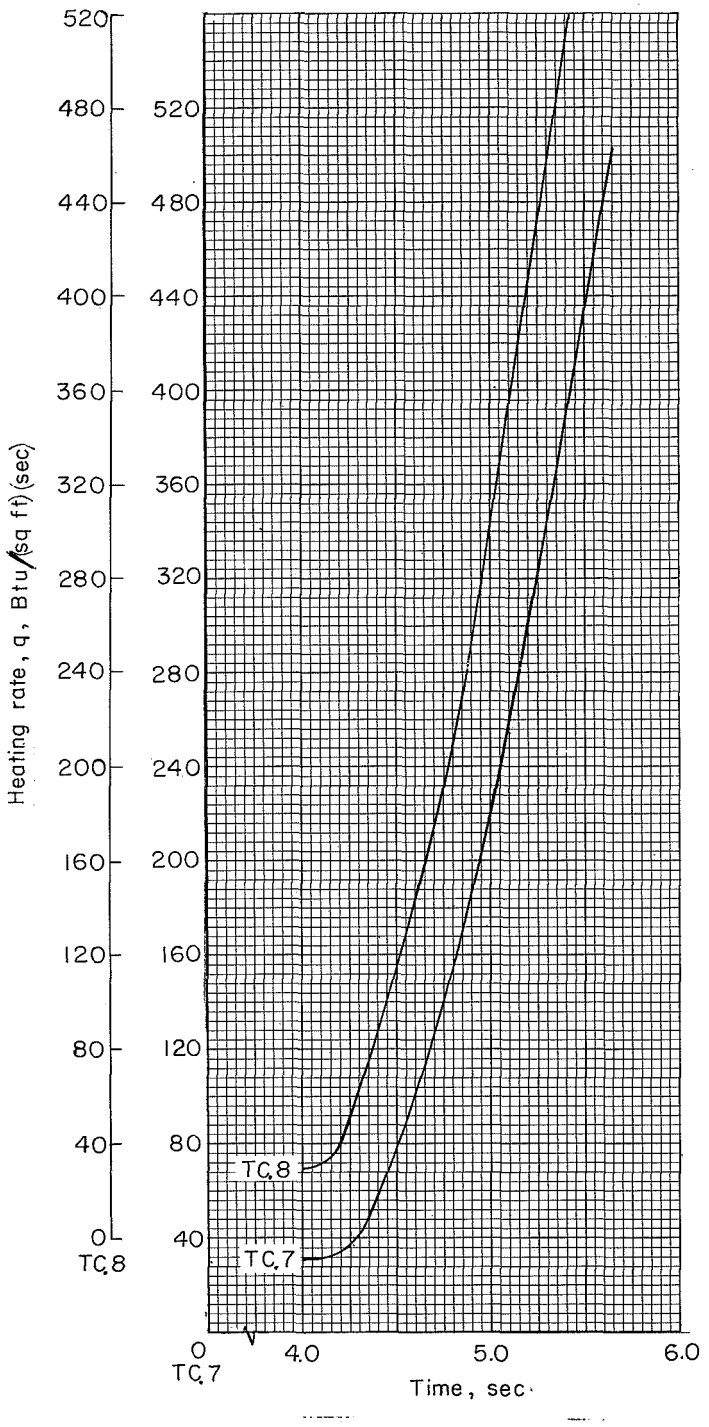

(c) Thermocouples 7 and 8.

Figure 9.- Continued.

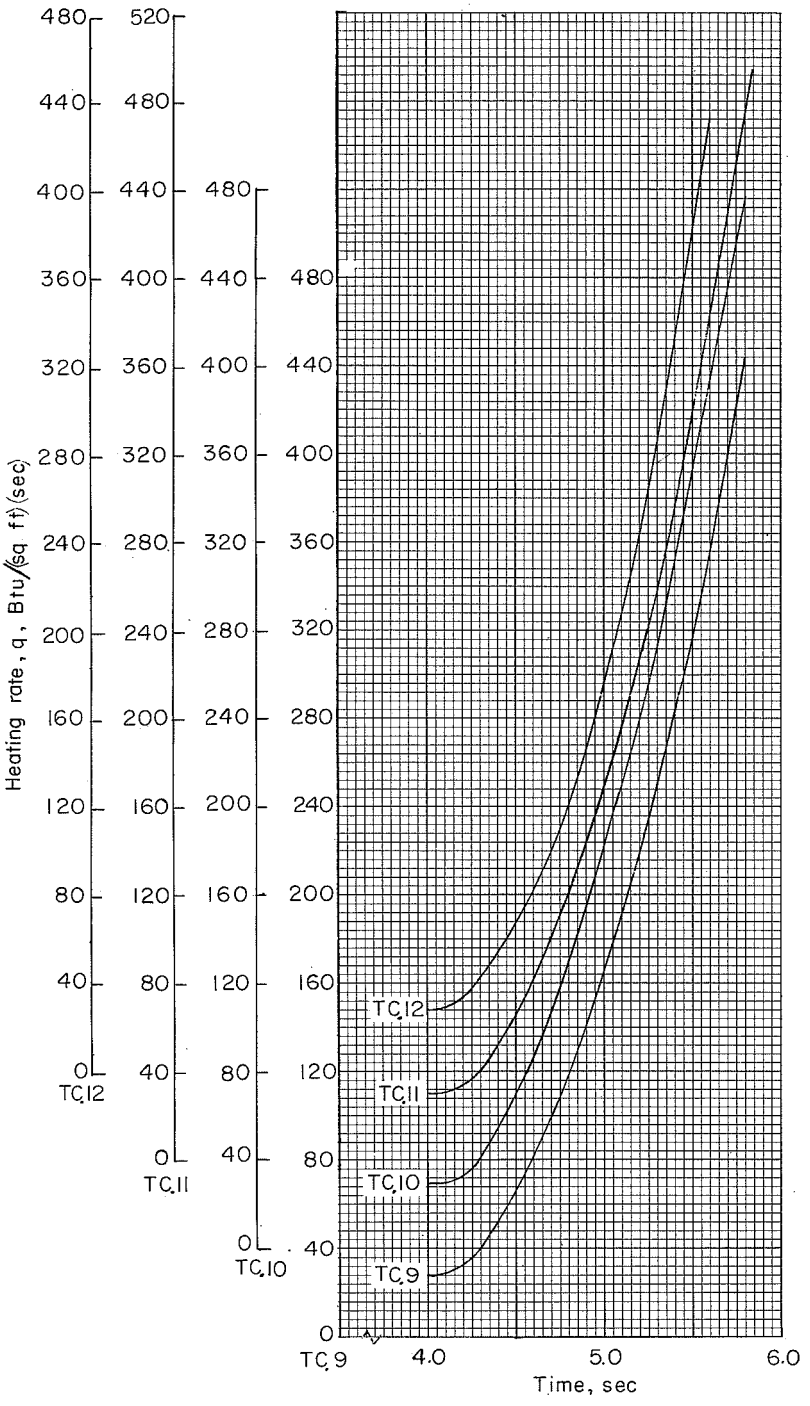

(d) Thermocouples 9 to 12.

Figure 9.- Continued.

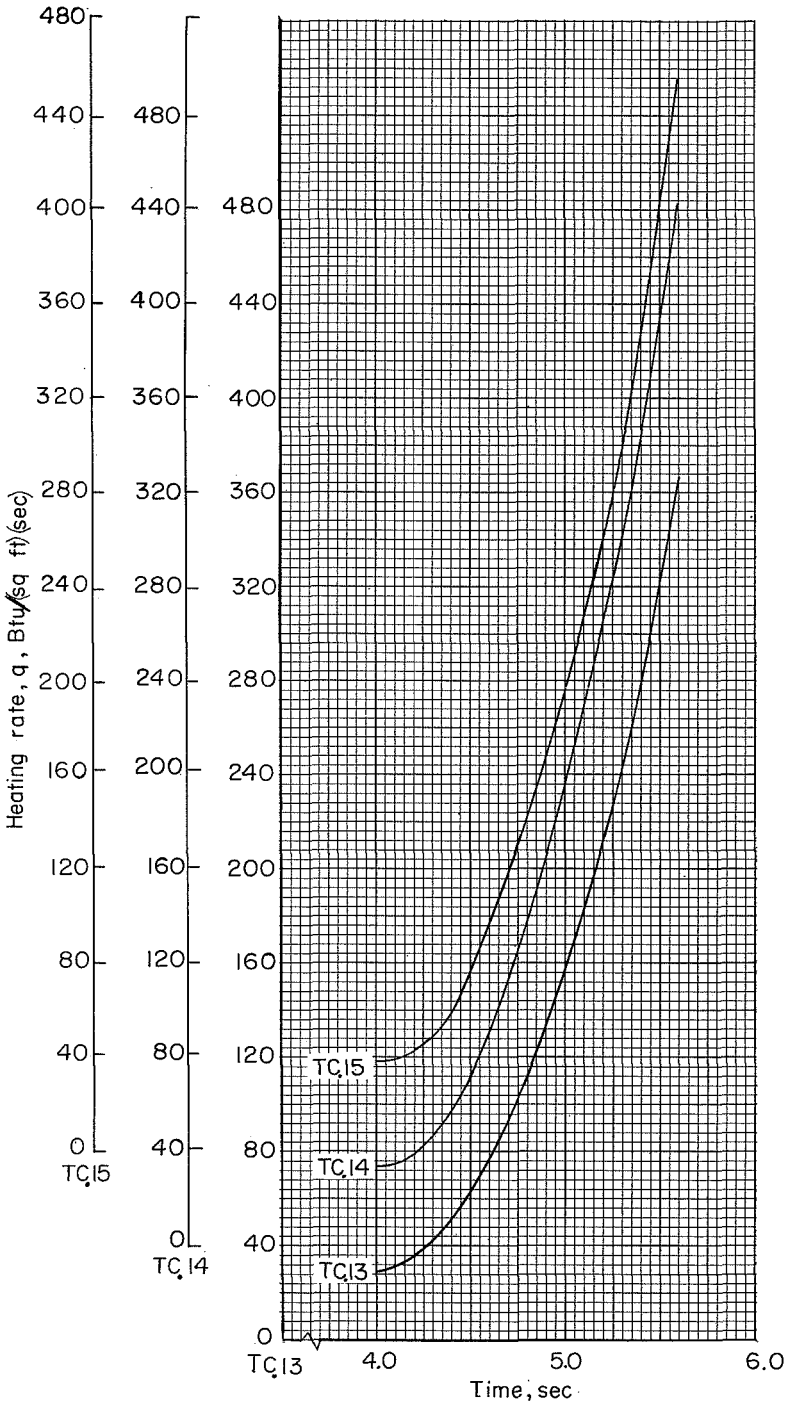

(e) Thermocouples 13, 14, and 15.

Figure 9.- Continued.

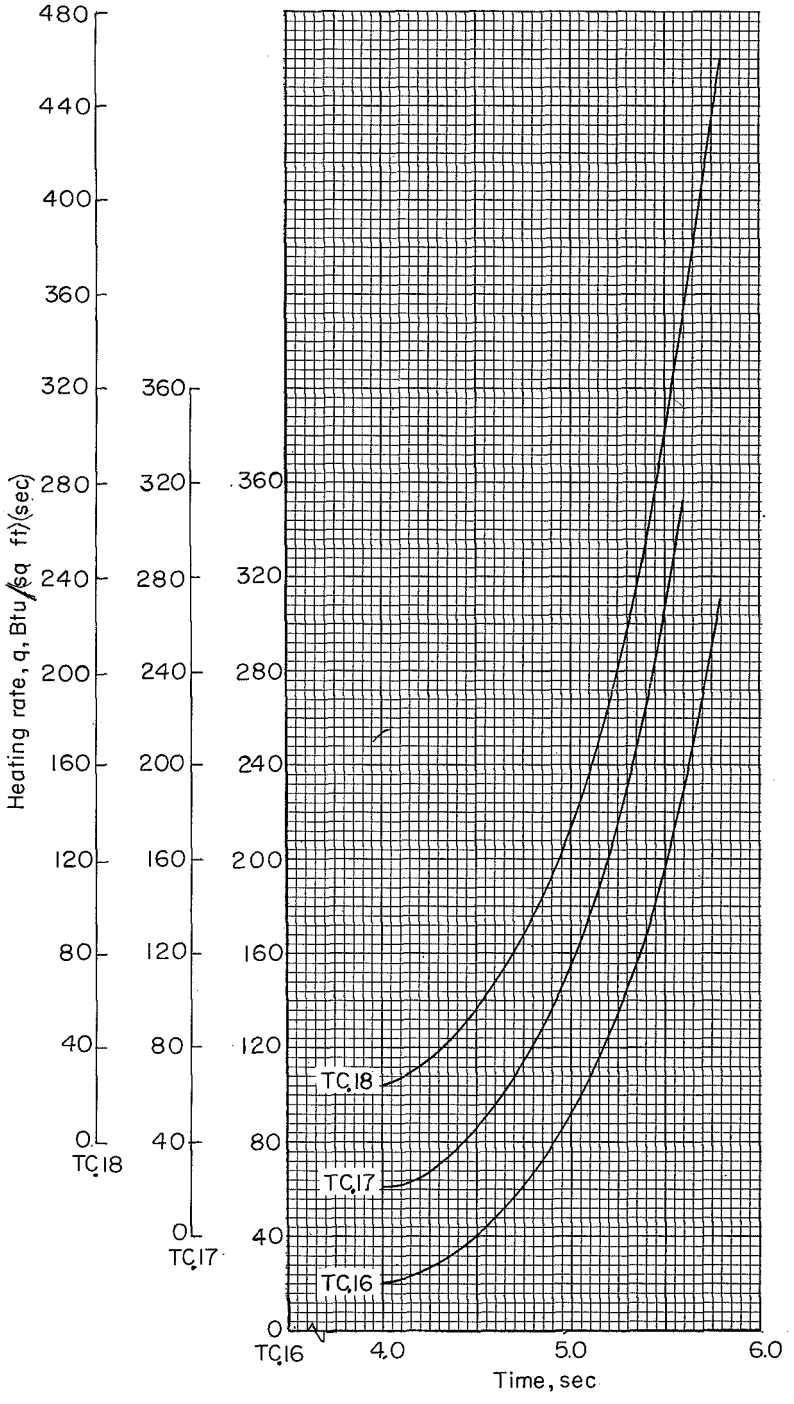

(f) Thermocouples 16, 17, and 18.

Figure 9.- Concluded.

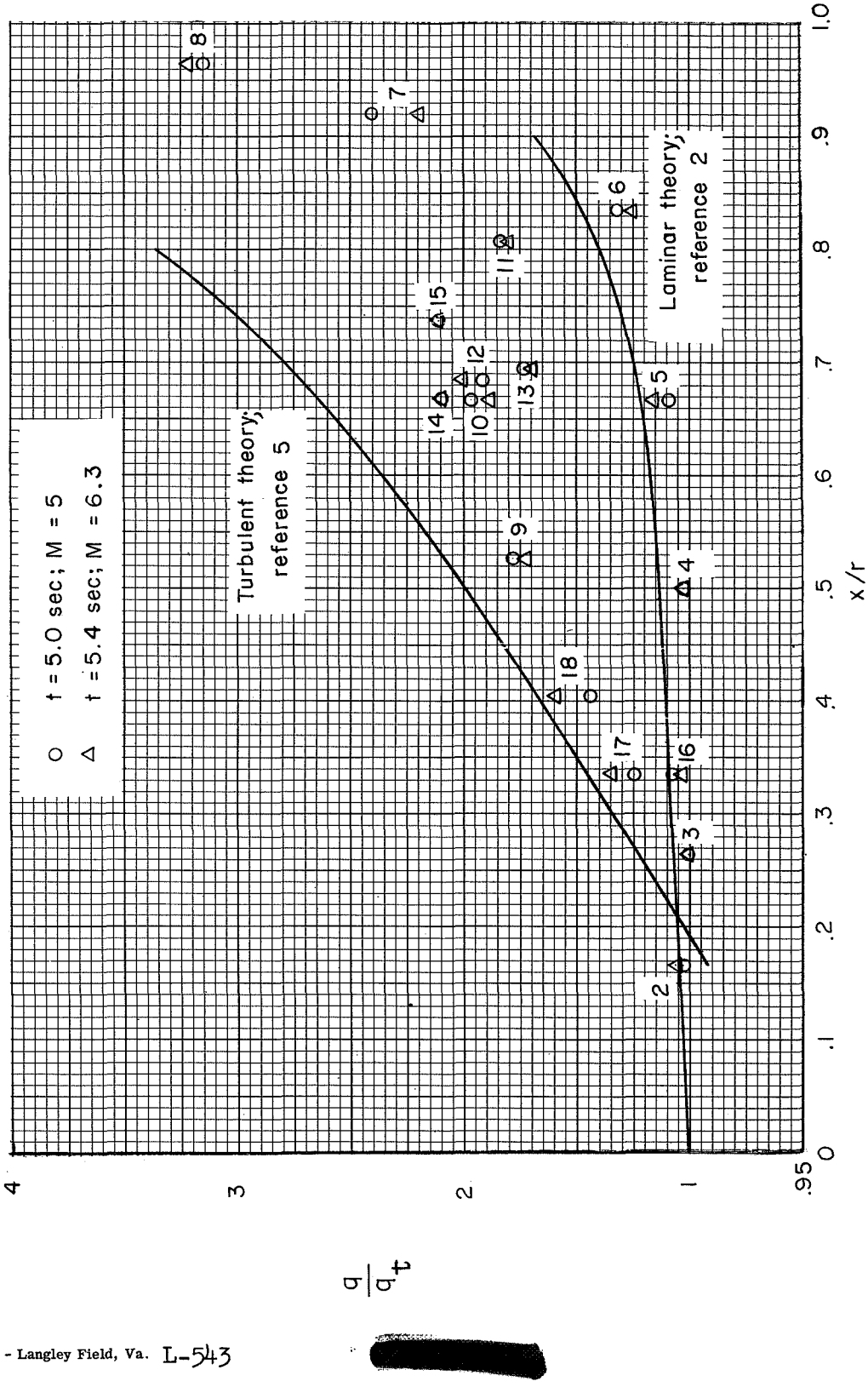

Figure 10.- Measured heating rates compared with theory.